Journal of Electronics and Electrical Engineering
https://ojs.wiserpub.com/index.php/JEEE

Research Article

Performance Characterizations of a Simultaneous "AND"-"OR" Gates System Dependent on a Parallel-Series SOA-MZIs Combination

Hassan Termos[1,2], Kassem Kallas[3,4*]

[1] ICFO—The Institute of Photonic Sciences, 08860 Castelldefels, Barcelona, Spain
[2] APEX Technologies, 91460 Marcoussis, France
[3] IMT Atlantique, Inserm UMR 1101, 29200 Brest, France
[4] National Institute of Health and Medical Research, Inserm UMR 1101, 29200 Brest, France
[*] Correspondence: kassem.kallas@imt-atlantique.fr

Received: 23 March 2026; **Revised:** 18 April 2026; **Accepted:** 22 April 2026; **Published:** 19 May 2026

Abstract: In this study, we experimentally investigate a simultaneous "AND"-"OR" all-optical logic gate system based on a series-parallel configuration of Semiconductor Optical Amplifier Mach-Zehnder Interferometers (SOA-MZIs). The proposed "AND" gate exploits the Cross-Phase Modulation (XPM) effect at the outputs of two parallel SOA-MZIs, while the "OR" gate, connected in series with the parallel stage, relies on Cross-Gain Modulation (XGM) in the third interferometer (SOA-MZI3). The system performance is evaluated in the optical, electrical, and temporal domains. Several performance metrics are considered, including power scaling, optical conversion efficiency, Optical Signal-to-Noise Ratio (OSNR), and Error Vector Magnitude (EVM), in order to characterize the generated optical "AND" and "OR" logic signals. Using an optical pulse source operating at 1550 nm with a pulse width of 1.3 ps and a repetition rate of 20 GHz, the proposed parallel-series SOA-MZI architecture produces up to 11 dBm of average output power with a conversion gain of 21 dB for the "OR" signal. At the SOA-MZI outputs, the maximum achievable bit rates for 64-QAM-modulated "AND" and "OR" signals reach 80 Gbit/s and 100 Gbit/s, respectively, at a common harmonic frequency of 80 GHz. The simultaneous logic gate system also demonstrates excellent optical performance, with optimal OSNR values of 61 dB for the "AND" signal and 82 dB for the "OR" signal. The generated "AND" and "OR" pulses exhibit temporal durations of 7.7 ps and 11.1 ps, respectively, at 1550 nm. In addition, the output beams show high spatial quality, with a beam-propagation factor $M^2 < 1.74$.

Keywords: all-optical "AND" and "OR" gates, Semiconductor Optical Amplifier Mach-Zehnder Interferometers (SOA-MZIs), Quadrature Amplitude Modulation (QAM)

1. Introduction

A wide range of applications, including radio-over-fiber, microwave, and cellular telecommunication systems, increasingly relies on all-optical logic circuits. Semiconductor Optical Amplifiers (SOAs), with their high gain and carrier-dependent refractive index changes, enable the realization of various all-optical logic gate functionalities. Owing to their favorable properties, SOA-based Mach-Zehnder Interferometers (SOA-MZIs) have been widely employed to implement all-optical logic gates [1–6] and wavelength converters [7–9]. Key features of SOA-MZIs include stability, compactness, simplicity, low input optical power requirements, high gain, and flexible integration with other photonic

DOI: https://doi.org/10.37256/jeee.5120269932

components. They also exhibit high Extinction Ratios (ER), signal regeneration capabilities, fast response times, and low chirp [10]. The inherent nonlinearity of SOA-MZIs makes them well-suited for digital optical signal processing, where Cross-Gain Modulation (XGM) and Cross-Phase Modulation (XPM) play a critical role in gate operation.

The SOA-MZI-based all-optical "AND" gate, a fundamental logic element, can perform bit-level operations for tasks such as address recognition, packet-header modification, and data synchronization and reliability enhancement [11]. Additionally, all-optical "XOR" gates, implemented using differential SOA-MZI architectures, can support high-speed operations up to 40 Gbit/s [12], enabling complex functions such as binary counting, addition, encoding, and cryptography. Combining fundamental gates "AND", "OR", "NAND", and "NOR" facilitates the implementation of arbitrary logical operations, which is essential for next-generation photonic communication networks that demand high speed, large capacity, and reliable performance [13].

Over the past two decades, significant research efforts have been devoted to the realization of all-optical logic gates using SOA-MZIs. These devices exploit the strong nonlinear properties of SOAs, such as XGM and XPM, to perform ultrafast optical signal processing without the need for optical-electrical-optical conversions. As a result, several logic gate functionalities, including "AND", "OR", "XOR", "NOR", and "NAND", have been experimentally demonstrated for Phase-Shift-Keying (PSK) modulated signals at bit rates exceeding 100 Gbit/s using SOA-MZI architectures [14–19]. In addition, previous work has shown that advanced gate operations can be realized by exploiting different control-signal configurations. For instance, an enhanced three-control-signal SOA-MZI architecture was previously proposed to realize a high-performance "AND" logic gate, demonstrating the capability of SOA-based interferometric systems to implement complex nonlinear optical operations [20]. Similarly, SOA-MZI-based architectures have also been investigated for the realization of high-speed "OR" logic gates, demonstrating the capability of such systems to support different logic functions under advanced operating conditions [21].

Despite these advances, most reported works focus on the realization of individual optical logic gates, where each gate function is implemented independently. However, future photonic communication and optical computing systems require more compact and multifunctional designs capable of performing multiple logical operations simultaneously while maintaining high processing speed and signal integrity. The realization of such multifunctional logic structures remains challenging because it requires careful control of nonlinear interactions within the interferometric structure while preserving signal quality at high modulation rates.

SOA-MZI-based all-optical logic gates have been extensively investigated, including both single-function and multifunctional configurations [22–24]. However, the reported approaches differ significantly in terms of architecture, modulation format, achievable bit rate, and level of experimental validation. In particular, prior multifunctional implementations are often limited to parallel configurations, reduced operating speeds, simplified signal formats, or lack comprehensive experimental characterization across multiple domains.

In this context, the present work focuses on the experimental demonstration and detailed characterization of a simultaneous "AND"-"OR" logic architecture based on a hybrid parallel-series SOA-MZI topology. In the proposed configuration, two parallel SOA-MZIs generate independent "AND" outputs, which are subsequently combined and injected into a third SOA-MZI operating in series to realize the "OR" function. This structure enables concurrent multi-function operation within a unified and scalable system.

Another important contribution of this work is the investigation of the proposed logic architecture under advanced modulation formats. Unlike most previous studies that rely on simple intensity-modulated signals or PSK formats, the present system operates with Quadrature Amplitude Modulation (QAM) signals. The use of high-order modulation formats is particularly relevant for modern high-capacity optical communication systems, where spectral efficiency and data throughput are critical design parameters. The proposed system enables high-speed signal processing at data rates of up to 100 Gbit/s, providing the practicality of developing complex optical logic functions for next-generation telecommunication networks.

In addition, the proposed system is investigated under 64-QAM modulation and evaluated in the optical, electrical, and temporal domains, providing a comprehensive assessment of its performance. Several key performance metrics are investigated, including Error Vector Magnitude (EVM), Optical Signal-to-Noise Ratio (OSNR), optical power scaling, and optical conversion efficiency. Furthermore, the influence of critical input parameters, such as wavelengths, repetition rates,

input data powers, and pulse widths, is systematically analyzed to determine their impact on the stability and performance of the concurrent logic operations. These investigations provide a deeper understanding of the nonlinear dynamics governing the SOA-MZI system and highlight the potential of the proposed architecture for high-speed all-optical signal processing applications. A quantitative comparison with representative SOA-MZI-based logic gate implementations is provided in order to clearly position the contribution of this work with respect to the state of the art.

2. Principle of operation

2.1 *Simultaneous "AND"-"OR" principle*

As illustrated in Figure 1, the "AND" gate is implemented using SOA-MZI1 and SOA-MZI2. In general, SOA-MZIs can function as optical switches, modulators, or sampling mixers [25–31]. In the proposed configuration, the SOA-MZIs are used simultaneously to realize both "AND" and "OR" gates with high performance. The SOAs in both arms of each interferometer are identical in terms of structure, material, and operating parameters.

To implement the Boolean operation $Q = A * B$ at the output of SOA-MZI1, the control signal B at frequency f_2 is injected into the middle port and equally split into the upper and lower arms of the interferometer. The data signal A at frequency f_1 enters the upper port. The output corresponding to the "AND" operation is extracted using an Optical Bandpass Filter (OBPF) centered at the wavelength of the control signal B. The resulting all-optical "AND" signal is generated through the combined effects of XGM and XPM, effectively performing the Boolean multiplication of A and B.

Specifically, the XPM effect in SOA1 causes the presence of signal A to induce a phase shift on signal B in the upper arm. When A is "ON," it modifies the SOA1 refractive index and carrier density, thereby inducing a phase change on B as it propagates through the interferometer. The output of SOA-MZI1 turns "ON" only when both A and B are "ON," and remains "OFF" if either input is "OFF." While the SOA-MZI1 output may amplify A or B individually, it does not produce the correct "AND" logic signal unless both inputs are active.

The second interferometer, SOA-MZI2, implements an identical "AND" operation, $Z = C * D$, with incoming data and control signals C and D. Both SOA-MZIs share the same design and operational parameters. Before combining the "AND" outputs via an Optical Coupler (OC) into SOA-MZI3, the wavelengths and frequencies of the input signals can be adjusted to characterize the "AND" signals in both optical and electrical domains.

In the SOA-MZI3 stage, no sampling or mixing is performed. The two "AND" signals, Q and Z, are combined at the lower port of the interferometer, although they could alternatively be injected at the upper port [28]. The amplified output is obtained after passing through the lower SOA (SOA6), realizing the "OR" gate, with Boolean operation $X = Q + Z$. It is important that the two "AND" signals share the same wavelength, so that the "OR" output matches the input wavelength. The "OR" output is "ON" in three cases: both Q and Z are "ON," Q is "ON" and Z is "OFF," or Q is "OFF" and Z is "ON".

Figure 1b shows the hypothetical electrical spectrum, which helps to illustrate the principle of the simultaneous "AND" and "OR" gates. In this configuration, the data signals A and C are identical, as are the control signals B and D. Consequently, the electrical spectra of A and C, as well as B and D, are the same. The harmonic amplitudes gradually decrease with increasing frequency, reflecting the short pulse width of the control signal, which behaves as a pulse train.

Since SOA-MZI1 and SOA-MZI2 share identical designs, operating points, and performance characteristics, the resulting "AND" signals Q and Z are also similar. Each "AND" signal is generated by multiplying the data and control signals of the corresponding SOA-MZI. Therefore, the power of each harmonic of Q or Z is the product of the corresponding harmonics of the data and control signals (e.g., $Q1 = A1 * B1, Z1 = C1 * D1$).

The "OR" signal X is obtained by combining Q and Z, resulting in harmonic components $Q1 + Z1$, $Q2 + Z2$, $Q3 + Z3$, and $Q4 + Z4$. The "OR" signal exhibits higher quality than the individual "AND" signals due to amplification provided by SOA6.

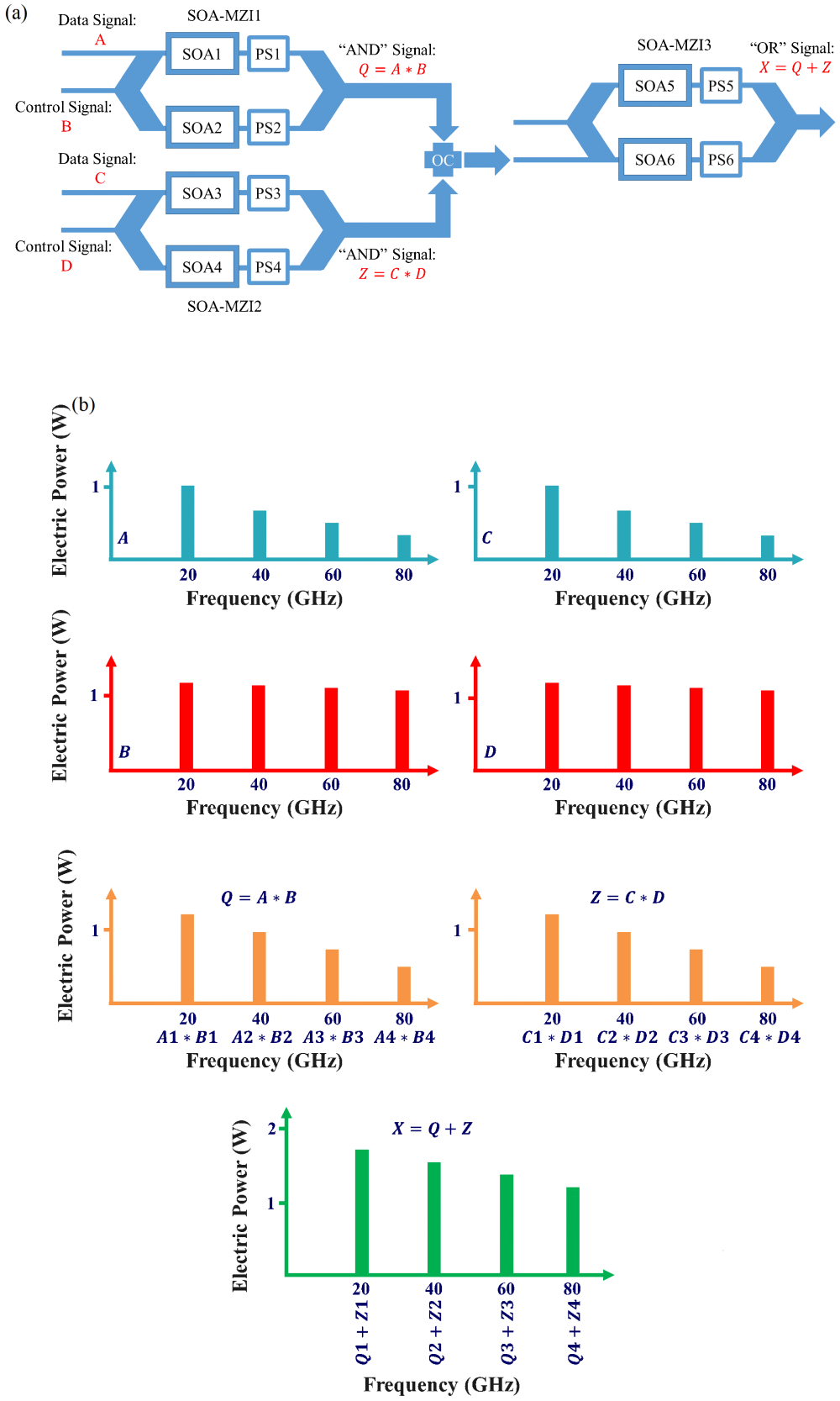

Figure 1. Simultaneous "AND" and "OR" principle (a) and hypothetical electrical spectrums (b)

2.2 *Theoretical background and physical interpretation of SOA-MZI-based "AND"-"OR" operations*

The operation of SOA-MZI-based optical logic gates is governed by the nonlinear interaction between optical signals and carrier dynamics in SOAs. The dominant mechanisms include gain saturation, XGM, and XPM [32–35]. The optical gain of the SOA follows a saturation behavior described by:

$$G = G_0/(1 + P_{\text{in}}/P_{\text{sat}}), \tag{1}$$

where G_0 is the small-signal gain, P_{in} is the input optical power, and P_{sat} is the saturation power. This relation reflects the gain compression effect caused by carrier depletion at high input power levels, which directly affects the signal amplitude and noise characteristics [32].

In addition to gain modulation, variations in carrier density induce changes in the refractive index through the linewidth enhancement factor, leading to a phase shift expressed as:

$$\Delta\phi \propto \Delta N \propto P_{\text{Control}}. \tag{2}$$

Where ΔN is the carrier density variation induced by the optical signal. This mechanism corresponds to XPM in SOA-MZI systems [28] that converts this phase variation into intensity modulation according to:

$$I_{\text{out}} \propto \cos^2(\Delta\phi/2), \tag{3}$$

where the output intensity depends on the phase difference between the two arms, highlighting the phase-sensitive nature of the interferometric process [34].

In the proposed architecture, the "AND" and "OR" operations are governed by fundamentally different physical mechanisms. The "AND" operation is primarily driven by XPM, where the presence of the control signal induces a phase shift that modifies the interference condition. The corresponding output can be expressed as:

$$I_{\text{AND,out}} \propto \cos^2(\Delta\phi/2). \tag{4}$$

This phase-sensitive behavior makes the "AND" signal highly dependent on carrier-induced refractive index changes and therefore more susceptible to phase noise and nonlinear distortions. At high bit rates, the finite carrier recovery time of the SOA limits its dynamic response, leading to increased phase distortion and degradation of signal quality [35].

In contrast, the "OR" operation is mainly governed by XGM, where the output intensity is directly controlled by the gain variation of the SOA. The output signal can be approximated as:

$$I_{\text{OR, out}} \propto G(P_{\text{CONTROL}})I_{\text{in}} \tag{5}$$

with:

$$G(P_{\text{CONTROL}}) = G_0/1 + P_{\text{CONTROL}}/P_{\text{sat}}. \tag{6}$$

This amplitude-based mechanism is less sensitive to phase fluctuations and interference conditions, resulting in improved robustness against nonlinear distortions and noise [32–35]. Furthermore, the additional amplification stage in the series SOA-MZI enhances the output signal power, contributing to higher OSNR and improved signal quality.

These fundamental differences provide a direct explanation of the experimental observations. The higher EVM values observed for the "AND" signal can be attributed to phase distortions induced by XPM, while the lower EVM of the "OR" signal results from the more stable amplitude modulation associated with XGM. Similarly, the improved OSNR and higher output power of the "OR" signal is consistent with the additional gain and reduced sensitivity to phase noise.

Finally, at higher bit rates, additional impairments such as gain saturation, finite carrier recovery dynamics, and pattern-dependent effects introduce further nonlinear distortions, which degrade signal quality and increase EVM. These effects are more pronounced in phase-sensitive operations such as "AND", while amplitude-based operations such as "OR" remain relatively more stable [32–35].

In the cascaded SOA-MZI configuration, the interplay between XPM and XGM plays a critical role in determining the overall system performance. The parallel stage generates the "AND" signal through XPM, resulting in a phase-modulated output, which is subsequently injected into the cascaded stage where XGM dominates to produce the "OR" output. This cascade introduces a coupling between phase and amplitude modulation processes.

At high repetition rates, the SOA operates in a quasi-steady-state regime, where the carrier density does not fully recover between successive pulses. This reduces carrier fluctuations and leads to more stable gain and phase conditions, which contributes to the good performance observed experimentally. Similar behavior has been reported in previous studies, where increasing the repetition rate improves signal stability due to carrier averaging effects and its Signal to Noise Ratio (SNR) [20, 21, 25].

However, this regime also introduces nonlinear memory effects such as gain saturation and pattern dependence, since the SOA response becomes dependent on the previous bit sequence. These effects may limit performance under more demanding conditions or higher data rates.

The impact of these dynamics differs between the two logic operations. The XPM-based "AND" signal remains more sensitive to phase variations and interferometric conditions, while the XGM-based "OR" signal benefits from a more stable amplitude response and improved robustness. These characteristics explain the good performance obtained for both signals at high repetition rates, while also highlighting potential limitations for system scalability.

3. Experimental setup

Figure 2 presents the experimental configuration employed to generate simultaneous "AND" and "OR" logic gate signals. The SOA-MZI devices used in this study are fabricated by the Center for Integrated Photonics (CIP) [36] and share identical structural characteristics, materials, and operational parameters, ensuring consistent performance across all stages of the system.

To realize the "AND" gate functionality, two interferometric structures, namely SOA-MZI1 and SOA-MZI2, are arranged in a parallel configuration. Each of these interferometers independently generates a high-quality "AND" output signal under identical operating conditions. The resulting "AND" signals are subsequently combined and injected into a third interferometer, SOA-MZI3, which is responsible for implementing the "OR" gate function.

In this configuration, the parallel stage dedicated to "AND" generation is effectively cascaded in series with SOA-MZI3 to achieve the "OR" operation. This hybrid series-parallel architecture enables the realization of a concurrent "AND"-"OR" logic gate system within a unified photonic platform. Such an arrangement offers a compact and efficient solution for performing multiple all-optical logic operations simultaneously.

Detailed investigations of the static and dynamic characteristics of the employed SOA-MZIs have been previously reported in [25–31]. In the present experiment, all SOAs are biased at a current of 400 mA to ensure stable and consistent operation.

An Optical Pulse Source (OPS) provided by Pritel Inc. is injected into the middle port of SOA-MZI1 and SOA-MZI2 [25, 37, 38]. This OPS is based on a mode-locked fiber laser, delivering ultra-short pulses with a repetition rate of $f_2 = f_4 = 20$ GHz, a pulse width of 1.3 ps, and a central wavelength of $\lambda_2 = \lambda_4 = 1550$ nm.

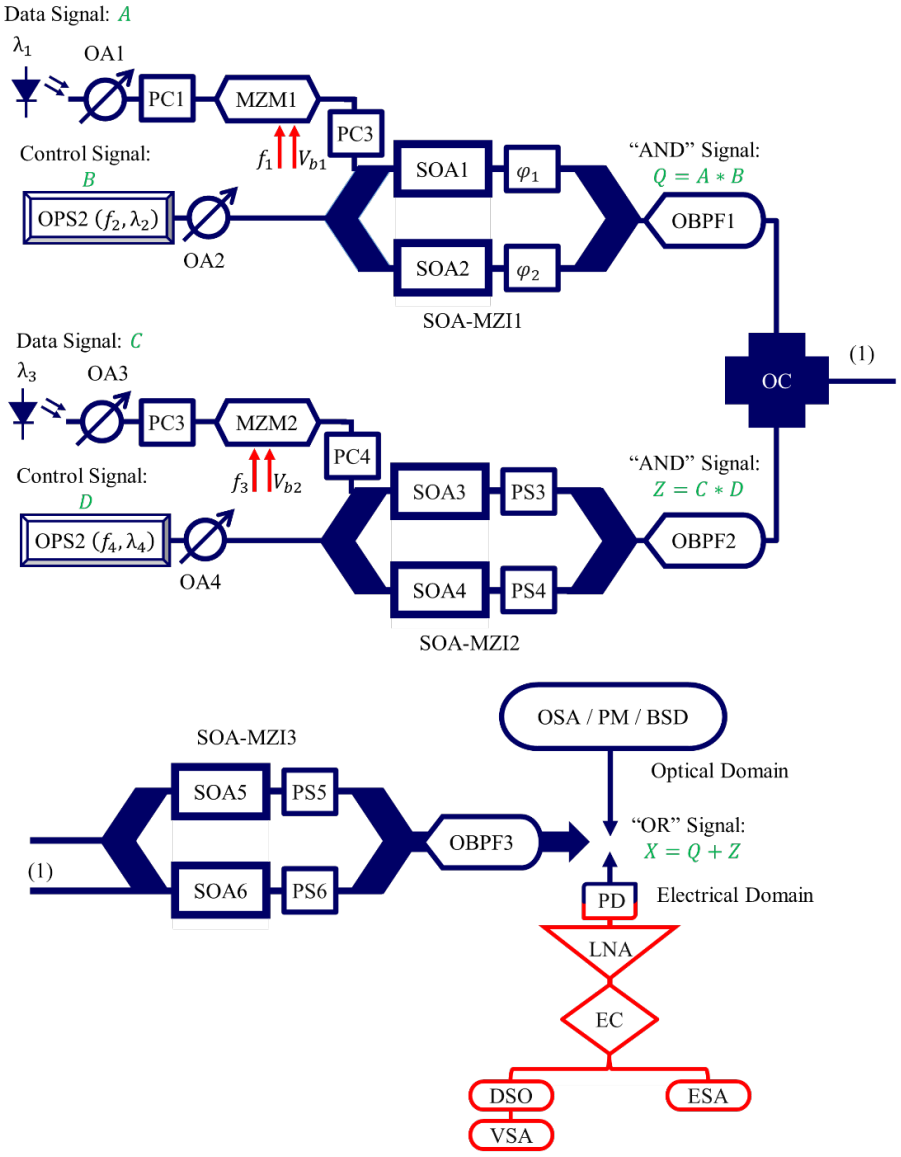

Figure 2. Experimental setup of the simultaneous "AND" and "OR" system. The dark blue paths represent optical devices, while the red paths indicate electrical ones

In parallel, an Arbitrary Waveform Generator (AWG) drives a Mach-Zehnder Modulator (MZM) to generate Quadrature Amplitude Modulation (QAM) data at the electrical domain. This signal is then imprinted onto an optical carrier and injected into the upper ports of SOA-MZI1 and SOA-MZI2. The resulting optical data signals operate at a frequency of $f_1 = f_3 = 20$ GHz, with a wavelength of $\lambda_1 = \lambda_3 = 1545$ nm. The input optical power is varied from -20 dBm to 5 dBm using Optical Attenuators (OA1 and OA3) to optimize the system performance.

The performance of the concurrent "AND"-"OR" architecture is evaluated at the outputs of the SOA-MZIs through comprehensive analysis in the temporal, optical, and electrical domains, enabling a complete characterization of the system efficiency and signal quality.

At the output of each SOA-MZI, the optical signal is spectrally filtered using an Optical Bandpass Filter (OBPF) centered at the wavelength of the OPS signal. This filtering stage plays a critical role in selecting the desired logic operation, ensuring that the interferometer output corresponds to either the "AND" or "OR" signal.

An OBPF bandwidth of 0.75 nm is carefully chosen to preserve the common frequency harmonics associated with the generated "AND" and "OR" signals, while effectively suppressing Amplified Spontaneous Emission (ASE) noise introduced by the SOAs. This trade-off enables high signal fidelity by maintaining the relevant spectral components and minimizing noise contributions.

The characterization of the "AND" and "OR" logic signals in the optical domain is performed using an Optical Spectrum Analyzer (OSA), while the average optical power is measured with a Power Meter (PM).

For electrical-domain analysis, the optical "AND" and "OR" signals are converted into their electrical counterparts using a high-speed Photodiode (PD). The resulting electrical signals measured by an Electrical Spectrum Analyzer (ESA) are subsequently amplified by a Low-Noise Amplifier (LNA) to enhance signal detectability and measurement accuracy.

The LNA provides a gain of 33 dB, ensuring sufficient amplification of the detected signals, whereas the PD exhibits a responsivity of 0.88 A/W and a bandwidth of 300 GHz along with low shot noise characteristics, enabling efficient optical-to-electrical conversion with minimal noise degradation.

To ensure the reliability of the experimental results, all measurements were repeated multiple times under identical operating conditions. The obtained results exhibited good reproducibility, with only minor variations observed between repeated measurements. The main experimental instruments, including OSA, ESA, PM, and PD, were calibrated prior to the measurements according to the manufacturer specifications.

The measurement uncertainties were estimated based on instrument accuracy and experimental repeatability. The uncertainty in optical power measurements is estimated to be within ±0.5 dB, while the uncertainty in OSNR evaluation is within ±1 dB. The temporal measurements present an uncertainty below ±0.2 ps, and the EVM measurements show a variation below ±0.5%. These uncertainty levels confirm the consistency and reliability of the reported experimental results.

The main experimental conditions and system parameters are summarized in Table 1 for clarity and reproducibility.

Table 1. List of experimental system parameters

Parameter	Value
Data signal wavelength	1545 nm
Modulation format	64-QAM
OPS repetition rate	20 GHz
Data frequency	20 GHz
OPS wavelengths	1550 nm
OPS pulse width	1.3 ps
SOA bias current	400 mA
Input optical power	−20 to 5 dBm
OPS average power	−11.7 dBm
OBPF bandwidth	0.75 nm
PD bandwidth	300 GHz
PD responsivity	0.88 A /W
LNA Gain	33 dB
Operating temperature	~25 °C

4. Optical pulse source characteristics

The quality of the generated "AND" and "OR" signals at the SOA-MZI outputs is significantly enhanced by the characteristics of the Optical Pulse Source (OPS). The OPS, employed as a control signal, operates at a repetition rate of $f_2 = f_4 = 20$ GHz.

As illustrated in Figure 3, the optical spectrum of the OPS is measured using an Optical Spectrum Analyzer (OSA) centered at a wavelength of 1550 nm. The OPS exhibits an average optical power of −11.7 dBm at its central wavelength and generates a pulse train with a Full Width at Half Maximum (FWHM) of 1.3 ps, enabling high temporal resolution.

For electrical-domain analysis, the optical signal is converted into an electrical signal using a PD followed by a LNA, as shown in Figure 4. The resulting electrical spectrum, measured with an ESA, consists of discrete harmonics at frequencies mf_2, where m is an integer representing the harmonic order. As expected, the amplitude of these harmonics decreases with increasing frequency.

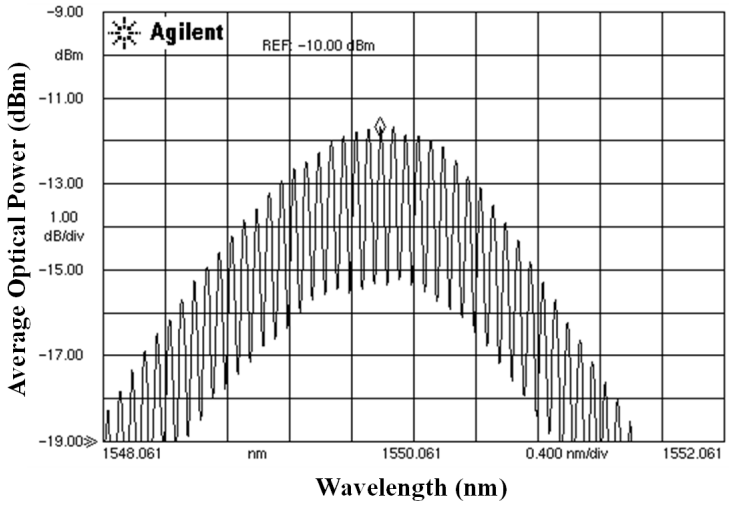

Figure 3. The optical signal of the used OPS

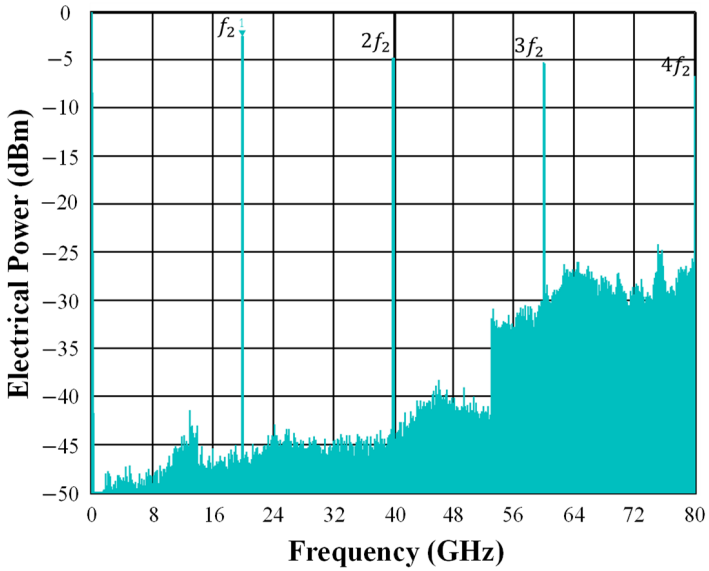

Figure 4. The electrical spectrum of the used OPS

However, due to the ultra-short pulse width of 1.3 ps, the spectral energy remains well distributed across higher-order harmonics, limiting their attenuation. Consequently, the power difference between the first and third harmonics remains within approximately 3 dB, indicating efficient harmonic generation and preservation.

5. SOA-MZI characteristics

The characteristics of the two semiconductor optical amplifiers (SOA1 and SOA2) employed in the SOA-MZI1 configuration (Figure 2) have been systematically investigated. Both SOAs are biased at a current of 400 mA to ensure stable operation. The optical gain is evaluated as a function of the input optical power by injecting a signal at a wavelength of 1550 nm into the SOA input.

As shown in Figure 5, the gain of both SOAs decreases with increasing input power due to gain saturation effects. Over the entire input power range, SOA2 consistently exhibits a higher gain than SOA1. At an input power of −30 dBm, the measured gains are 27 dB for SOA1 and 29 dB for SOA2. The saturation powers, defined at a 3 dB reduction from the maximum gain, are approximately −13 dBm for SOA1 and −12 dBm for SOA2. It is important to note that the generated "AND" and "OR" signals at the SOA-MZI outputs are centered at a wavelength of 1550 nm, ensuring compatibility with the SOA gain peak.

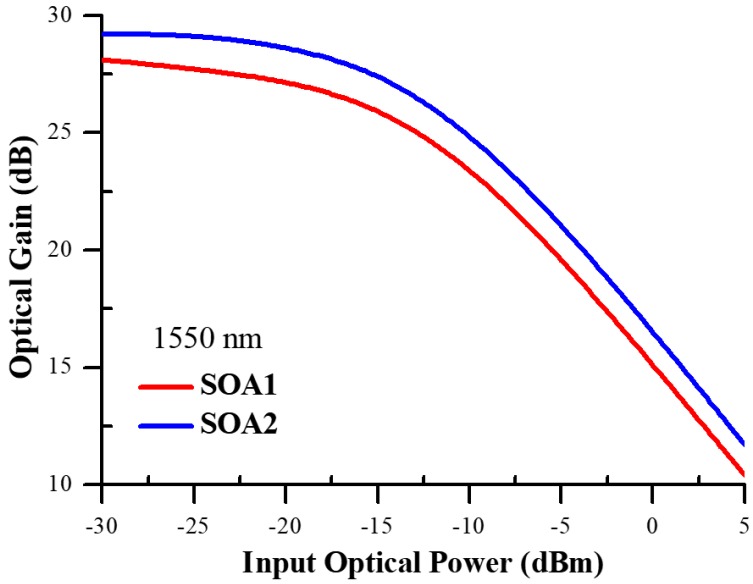

Figure 5. SOAs characteristic at the wavelength of 1550 nm

The Extinction Ratio (ER) is defined as the power difference between the "ON" and "OFF" states of the output signal. The "ON" state corresponds to a high transmission level achieved under appropriate control signal conditions, whereas the "OFF" state represents a low transmission level. The ER is evaluated for input data powers ranging from −20 dBm to −5 dBm, providing a quantitative measure of the logic gate performance of the SOA-MZI.

To determine the optimal operating conditions for achieving high-performance "AND" and "OR" gate functionalities, a systematic calibration procedure of the SOA-MZIs is implemented. The bias current of SOA1 is fixed at 400 mA, while the phase shifters PS1 and PS2 are adjusted to minimize the output optical power in the absence of the control signal. This condition ensures proper interferometric balance and maximizes the ER.

Subsequently, the bias current of SOA2 is finely tuned to further reduce the residual output power, while maintaining SOA1 at a constant bias of 400 mA. The optimization process involves a simultaneous adjustment of the SOA2 bias current

and the phase shifters PS1 and PS2. An optimal operating point is achieved when SOA2 is also biased at 400 mA, resulting in the minimum average output power and, consequently, an enhanced ER at the SOA-MZI output.

The data signal is injected into the upper port of the SOA-MZI at a wavelength of 1545 nm, with its input power varied over a defined range. Meanwhile, the control signal at 1550 nm is applied with an input power ranging from −40 dBm to 10 dBm, significantly influencing the output signal characteristics. As shown in Figure 6, the SOA-MZI exhibits a maximum ER of 23 dB at an input data power of −10 dBm, indicating the optimal operating point. The highest ER is obtained for a control signal peak power of approximately −3 dBm, corresponding to the OPS signal conditions illustrated in Figure 2.

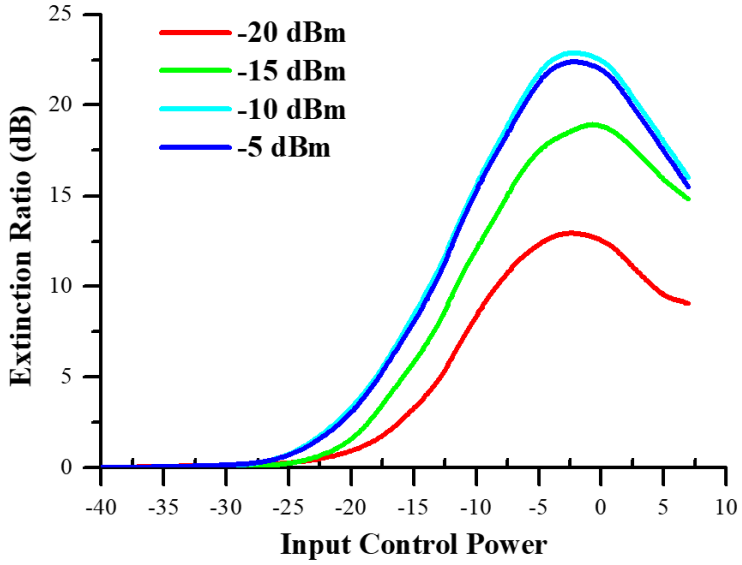

Figure 6. SOA-MZI characteristic with different ERs at the SOA-MZI output for different input data powers

Figure 6 also presents the variation of the ER as a function of input data power measured in dBm, ranging from −20 dBm to −5 dBm in 5 dB steps, confirming that the optimal performance is achieved at −10 dBm. It is important to note that the peak power (P_p) of the OPS signal can be derived from its average power (P_{av}) using the relation:

$$P_p = P_{av}/\alpha \tag{7}$$

where the duty cycle α is defined as:

$$\alpha = \Delta * t\, f_2 = \Delta * t\, f_4. \tag{8}$$

For a pulse width $\Delta t = 1.3$ ps and repetition rate of 20 GHz, the duty cycle is approximately 2.6%.

Finally, it should be emphasized that the power of the central spectral component observed in Figure 3 does not represent the true average power of the OPS signal. The accurate average power is measured directly using a Power Meter (PM) prior to injection into the SOA-MZI inputs.

6. Power scaling measurements

Power-scaling characteristics of the "AND" and "OR" signals are evaluated at the outputs of SOA-MZI1 and SOA-MZI3, respectively, as illustrated in Figure 7.

Figure 7a presents the output power of the "AND" signal at the SOA-MZI1 output as a function of the input data power, along with the corresponding optical conversion gain. A maximum output power of approximately 1 dBm is achieved at an input data power of −10 dBm, corresponding to a conversion gain of 11 dB. This result is consistent with the optimal operating point identified in Figure 6, where the SOA-MZI exhibits its best performance.

A similar analysis is performed for the "OR" signal at the SOA-MZI3 output, as shown in Figure 7b. The experimental results indicate a maximum output power of 11 dBm at an input data power of −10 dBm, corresponding to a significantly higher conversion gain of 21 dB. This demonstrates the enhanced efficiency of the "OR" stage within the proposed concurrent "AND"-"OR" architecture.

The superior performance of the "OR" signal can be attributed to the additional amplification provided by SOA6 in the SOA-MZI3 stage, whose gain characteristics are comparable to those of SOA2 as seen in Figure 5. As a result, both the output power and conversion gain of the "OR" signal are substantially higher than those of the "AND" signal generated at the SOA-MZI1 stage. This improvement is particularly pronounced at lower input data power levels, where the impact of amplification is more significant.

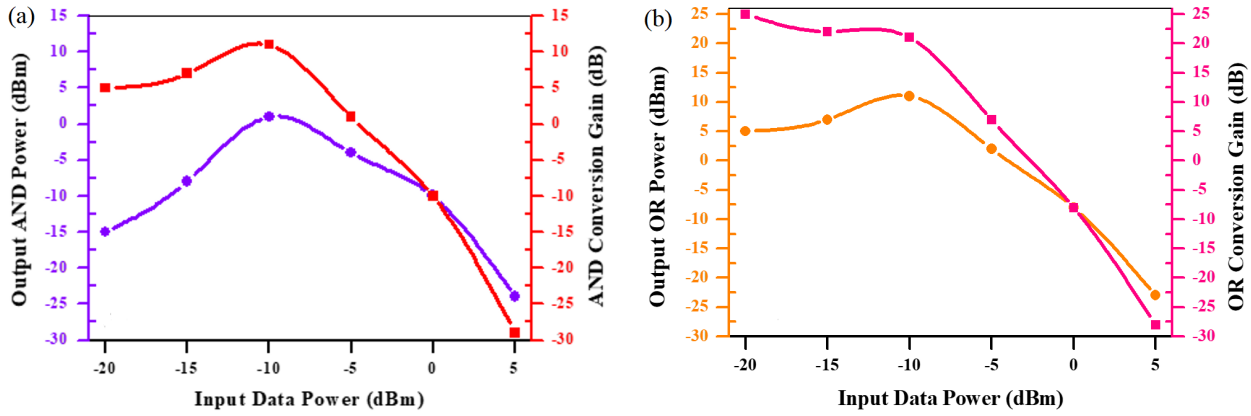

Figure 7. Power scaling characteristics of (a) the "AND" signal at the SOA-MZI1 output and (b) the "OR" signal at the SOA-MZI3 output

7. Optical signal to noise ratio

Optical Signal-to-Noise Ratio (OSNR) is a key performance metric in a wide range of applications, including RoF, microwave photonics, and wireless communication systems. It is defined as the ratio of signal power to noise power, or equivalently as the difference between signal and noise levels expressed in dBm within a specified optical bandwidth. The OSNR performance of the simultaneous "AND"-"OR" system is presented in Figure 8 for the outputs of SOA-MZI1 and SOA-MZI3, corresponding to the "AND" and "OR" signals, respectively as a function of the input optical power measured in dBm. At an input data power of −10 dBm, the "AND" signal achieves a maximum OSNR of 61 dB, while the "OR" signal reaches a significantly higher value of 82 dB.

This enhancement in the "OR" signal OSNR can be attributed to the additional amplification provided by SOA6 in the lower arm of SOA-MZI3, along with its intrinsic gain characteristics. As a result, the "OR" signal generally exhibits improved OSNR, particularly at lower input data power levels [25]. It is also worth noting that the corresponding optical signal powers for both "AND" and "OR" outputs are presented in Figure 7.

It is worth noting that the reported OSNR values correspond to measurements performed under controlled laboratory conditions, where the system is optimized in terms of input power levels, optical filtering, and limited propagation losses.

In particular, the use of a narrow optical bandpass filter contributes to reducing the impact of noise and enhancing the measured OSNR.

In practical implementations, the OSNR is expected to be lower due to several factors, including ASE noise accumulation in the SOAs, cascading stages, insertion losses, and fiber propagation effects. Therefore, the reported values should be considered as an upper-bound performance under optimized experimental conditions. This consideration provides a more realistic interpretation of the system performance in real-world applications.

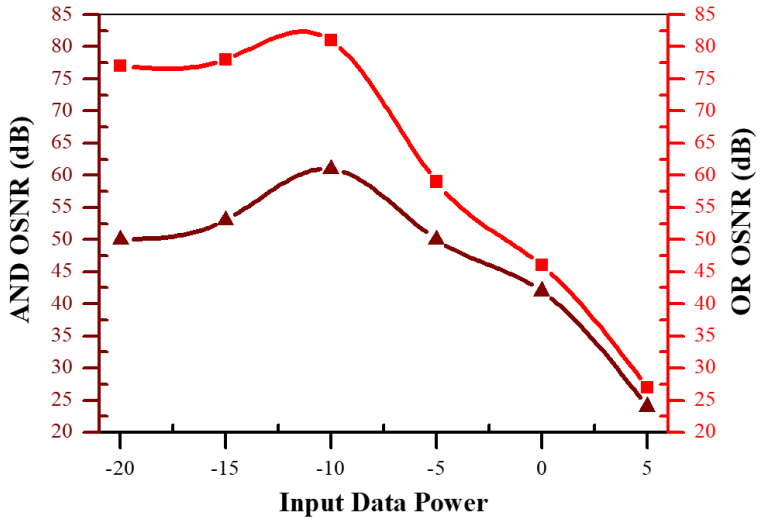

Figure 8. OSNRs of the "AND" signal at the SOA-MZI1 output and the "OR" signal at the SOA-MZI3 output

8. Spatial beam quality

The beam quality factor (M^2), presented in Figure 9, also referred to as the Beam Propagation Ratio (BPR), is a fundamental parameter for evaluating laser beam quality. It is a dimensionless quantity that quantifies the deviation of a real laser beam from an ideal fundamental Gaussian mode (TEM00), for which $M^2 = 1$. Consequently, the M^2 parameter determines the ability of the beam to be tightly focused, with lower values indicating superior beam quality and better spatial coherence.

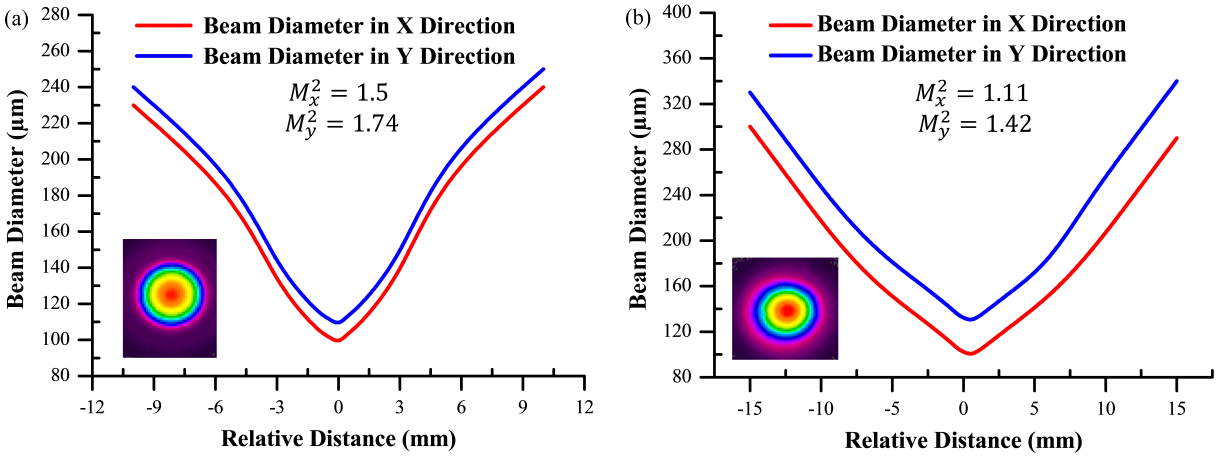

Figure 9. Spatial beam profile and M-squared beam quality measurements of the "AND" (a) and "OR" (b) signals

The M^2 values along the X and Y transverse directions are calculated using standard analytical expressions based on beam propagation theory [39, 40], as given below:

$$M^2{}_x = \pi D_{2\min.x}/2\lambda * 2Z_{r,x} \tag{9}$$

$$M^2{}_y = \pi D_{2\min.y}/2\lambda * 2Z_{r,y}. \tag{10}$$

Where $Z_r = |Z_{\max} - Z_{\min}|/2$ is the Rayleigh length, $\lambda = \lambda_2 = \lambda_4$ is the wavelength of the laser beam of the "AND" and "OR" signals, $D_{\min}$ is the beam diameter at the beam waist, $Z_{\max}$ corresponds to the distance along the beam propagation where the beam diameter is 1.414 $D_{\min}$, and $Z_{\min}$ corresponds to the distance along the beam propagation on the other side of the beam where the beam diameter is also 1.414 $D_{\min}$.

The spatial beam profile along X and Y directions of the "AND" signal at the SOA-MZI1 output at a central wavelength of 1550 nm, which is measured using a pyroelectric camera, is shown in Figure 9a, emphasizing a single-peak Gaussian distribution and outstanding circularity of 95%. The output SOA-MZI signal from the fiber is collimated before being coupled into a free-space beam-squared device. The beam diameter of the "AND" signal over the Rayleigh range is measured using a lens that has a focal length of 100 mm and a scanning beam profiler. By analyzing the variation of the obtained beam diameter, the spatial beam quality parameters that are M^2 ones are estimated to be $M^2{}_x = 1.5$ and $M^2{}_y = 1.74$ for the "AND" signal, as shown in Figure 9a.

Analogous to the measurements, the spatial beam profile of the "OR" signal at the SOA-MZI3 output at 1550 nm is presented in Figure 9b, which also affirms a single-peak Gaussian distribution with a circularity of 92%. The beam M-squared of the "OR" signal in this condition is measured to be $M^2{}_x = 1.11$ and $M^2{}_y = 1.42$. As a result, the "OR" output beam has excellent quality and efficiency, as mentioned in its OSNR in Figure 8 at the SOA-MZI3 output; which explains the superior M^2 values compared to those of the "AND" signal at the SOA-MZI1 output.

9. Electrical "OR" spectrum

Figure 10 presents the electrical characterization of the "OR" gate at the SOA-MZI3 output. In this measurement, the electrical output power is analysed at frequencies corresponding to the repetition rate of the OPS signal, providing a direct representation of the "OR" gate operation.

The results confirm the effectiveness of the parallel-series SOA-MZI architecture in implementing the "OR" function. In this configuration, the first two input signals are applied to SOA-MZI1 to generate the first "AND" output, while the remaining two signals are injected into SOA-MZI2 to produce the second "AND" output. These two "AND" signals are then combined and fed into SOA-MZI3, resulting in the electrical "OR" signal at its output.

The electrical "OR" signal, obtained by combining the two independent "AND" signals from SOA-MZI1 and SOA-MZI2, exhibits a rich harmonic structure. The signal contains multiple harmonics at frequencies defined by $H_m = mf_2$, where m is the harmonic order and f_2 is the repetition rate of the control pulses.

Notably, the fourth harmonic at $H_4 = 4f_2 = 80$ GHz represents the maximum frequency supported by the proposed simultaneous "AND"-"OR" system, while the fundamental harmonic occurs at $H_1 = f_2 = 20$ GHz. The power difference between these two harmonics is approximately 10 dB, indicating a moderate roll-off in harmonic amplitude as frequency increases. This behaviour reflects the high-fidelity temporal shaping and spectral quality of the generated "OR" signal.

The ER of the electrical "OR" signal is evaluated at the output of SOA-MZI3. By definition, the ER corresponds to the difference between the maximum and minimum electrical power levels of the signal, providing a measure of signal contrast and logical fidelity.

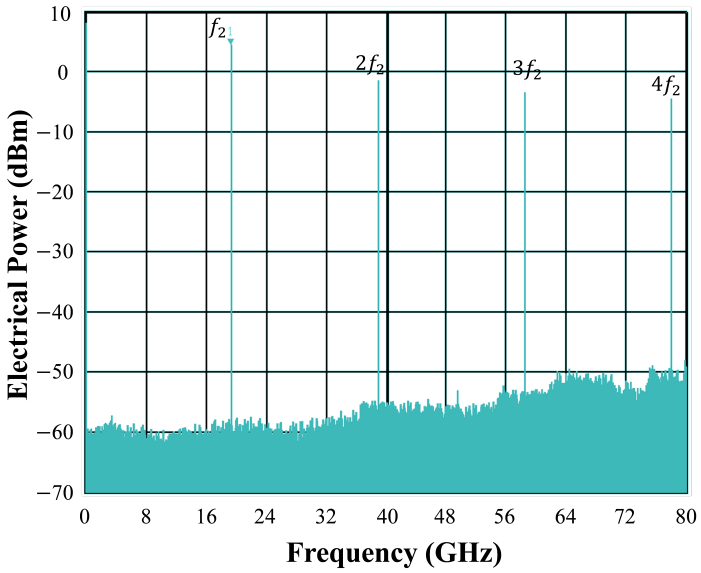

Figure 10. Electrical spectrum of the "OR" signal after filtering, photodetection, and amplification

As shown in Table 2, the "OR" signal achieves an ER of 44 dB at the fourth harmonic frequency of 80 GHz, whereas the ER at the fundamental frequency of 20 GHz is even higher, approximately 65 dB. These results demonstrate that the system maintains excellent signal contrast across a wide frequency range, highlighting the effectiveness of the series-parallel SOA-MZI architecture in generating high-quality simultaneous logic operations.

Table 2. ER of the "OR" signal at the SOA-MZI3 exit

Harmonic frequency (GHz)	ER (dB)
20	65
40	54
60	50
80	44

10. Error vector magnitude

Several key performance metrics, most notably the Error Vector Magnitude (EVM) at the SOA-MZI outputs, are employed to characterize the proposed concurrent photonic "AND"-"OR" network, as shown in Figure 11. The concept and significance of EVM are described in detail in [41]. In the experiment, the optical inputs to SOA-MZI1 and SOA-MZI2 carry 64-QAM (quadrature amplitude modulation) data. The 64-QAM electrical signals are generated by an AWG at a repetition frequency of $f_2 = f_4 = 20$ GHz and applied to the electrical port of an optical Mach-Zehnder modulator (MZM) to encode the data onto the optical carrier.

The measured EVM values are used to assess the quality of the "AND" outputs from SOA-MZI1 and SOA-MZI2, as well as the "OR" output from SOA-MZI3. To facilitate accurate digital evaluation, the optical "AND" and "OR" signals are converted into the electrical domain and recorded using a Digital Sampling Oscilloscope (DSO). The 64-QAM EVM is subsequently calculated using a Vector Signal Analyzer (VSA) over a range of bit rates from 1 to 100 Gbit/s.

As shown in Figure 11, the 64-QAM-modulated "AND" and "OR" signals are generated at two harmonic frequencies, 20 GHz and 80 GHz, corresponding to the common frequencies of the system. For the concurrent optical "AND-OR"

network, the measured 64-QAM EVM remains below 8% [42]. Furthermore, the overall system transmission performance can be enhanced by applying Forward Error Correction (FEC) techniques [43, 44] during the demodulation of the 64-QAM "AND" and "OR" signals.

Figure 11 presents the EVM of the 64-QAM "AND" and "OR" signals at the outputs of the SOA-MZIs as a function of bit rate and harmonic frequency. The EVM for both signals increases with higher bit rates and harmonic orders. Specifically, Figure 11a shows that the EVM of the "AND" signal rises from 2.5% to 8% at 20 GHz, whereas the "OR" signal exhibits a smaller increase, from 2% to 4%. This indicates that, at higher bit rates, the "OR" signal maintains superior performance relative to the "AND" signal.

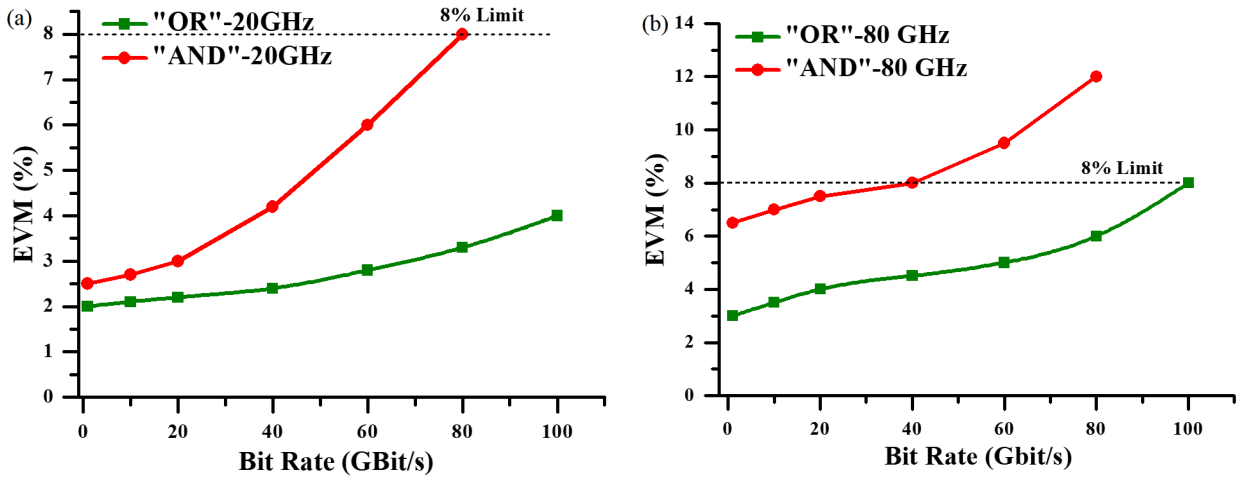

Figure 11. EVMs of the "AND" and "OR" signals at the SOA-MZI1 and SOA-MZI3 outputs, respectively, at 20 GHz (a) and 80 GHz (b) versus the bit rate

The maximum achievable bit rates are 100 Gbit/s for the "OR" signal and 80 Gbit/s for the "AND" signal, reflecting the enhanced amplification provided at the SOA-MZI3 output for the "OR" stage. In Figure 11b, the EVM of the "AND" signal exceeds its acceptable threshold at 80 Gbit/s, reaching 12%, while the "OR" signal remains below 8% even at 100 Gbit/s. This demonstrates that the "OR" operation maintains improved signal fidelity across the entire bit rate range. All EVM measurements are performed with an input data power of −10 dBm at the SOA-MZI inputs.

The observed EVM behavior can be explained by considering the nonlinear dynamics of the SOA-MZI system. In the case of the "AND" operation, the signal generation is strongly influenced by XPM, which induces phase distortions due to carrier-induced refractive index variations. These phase distortions increase with input power and bit rate, leading to a degradation of signal quality and higher EVM values.

In contrast, the "OR" operation is mainly governed by XGM, which is an amplitude-based mechanism and is generally less sensitive to phase noise. As a result, the "OR" signal exhibits improved robustness and lower EVM compared to the "AND" signal.

Furthermore, additional system impairments contribute to EVM degradation at higher bit rates, including gain saturation, carrier recovery dynamics, pattern-dependent effects, and harmonic distortion. These effects become more pronounced at higher frequencies, explaining the increase of EVM with bit rate and harmonic order observed in the experimental results.

It is important to emphasize that SOA-MZI-based systems are inherently affected by noise accumulation and pattern-dependent effects, which are important considerations for practical deployment in Photonic Integrated Circuits (PIC). ASE noise generated in SOAs contributes to OSNR degradation and may accumulate in cascaded configurations. This effect becomes more significant as the number of stages increases [45–47].

In addition, the finite carrier recovery time of the SOA introduces pattern-dependent behavior, where the system response depends on the preceding bit sequence. This results in nonlinear memory effects that can distort both amplitude and phase of the signal, especially at high bit rates.

In the present work, these effects remain limited due to the optimized operating conditions, including controlled input power levels and a relatively small number of cascaded stages. This is consistent with the good OSNR and EVM performance observed experimentally. However, for larger-scale systems or higher data rates, noise accumulation and pattern dependence may become dominant factors limiting performance and scalability.

11. Temporal characterizations

Temporal characterization of the logic gate outputs was performed using a high-speed oscilloscope to measure the pulse width of both the "AND" signal at the SOA-MZI1 output and the "OR" signal at the SOA-MZI3 output as displayed in Figure 12.

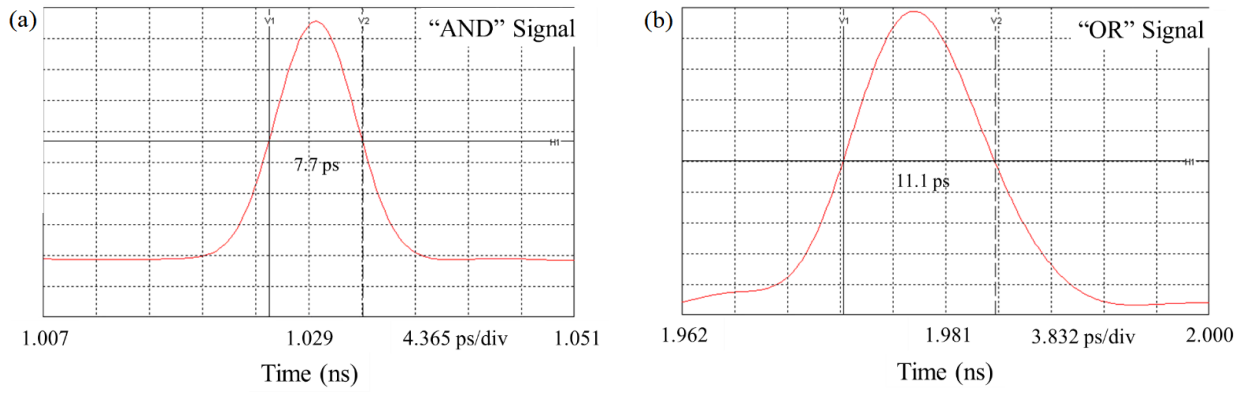

Figure 12. The waveforms of the "AND" signal (a) and "OR" signal (b)

The "AND" pulse exhibits a FWHM of 7.7 ps (Figure 12a), which corresponds to approximately 5.9 times the duration of the input optical pulse from the OPS.

Similarly, the "OR" pulse displays a Gaussian-shaped waveform with an FWHM of 11.1 ps (Figure 12b), exceeding the "AND" pulse width and representing an 8.5-fold broadening relative to the 1.3-ps input OPS pulse. Notably, the "OR" signal demonstrates higher optical power and lower noise compared to the "AND" signal, which can be attributed to the additional amplification provided by the series SOA-MZI3 stage.

These results indicate that the proposed system successfully preserves short pulse durations for both "AND" and "OR" outputs, while achieving enhanced optical quality for the "OR" signal. All temporal measurements were conducted with an input data power of −10 dBm applied to the inputs of both SOA-MZI1 and SOA-MZI2.

12. Comparison of SOA-MZI-based logic gate architectures

As shown in Table 3, previous works have primarily focused on either single-function logic gates or multifunctional architectures with certain limitations, such as reduced operating speed, simplified modulation formats, or lack of experimental validation. In particular, recent studies have demonstrated advanced "AND" and "OR" gate designs based on SOA-MZI configurations, but these remain restricted to individual logic functions or theoretical analyses.

In contrast, the present work combines simultaneous "AND"-"OR" operation within a hybrid parallel-series SOA-MZI topology and validates its performance experimentally under 64-QAM modulation. Furthermore, the system is characterized

in the optical, electrical, and temporal domains, providing a more complete evaluation compared to existing approaches. This combination of simultaneous functionality, experimental validation, advanced modulation, and multi-domain analysis defines the specific contribution of the proposed system.

In addition to the functional comparison presented in Table 3, a practical comparison in terms of energy efficiency, footprint, and cascadability is provided in Table 4.

Table 3. Comparison of representative SOA-MZI-based optical logic gate implementations

Ref.	Architecture	Logic frunctions	Validation	Modulation	Bit rate (Gbit/S)
[22]	Single SOA-MZI differential	"AND"	Experimental	Optical logic	80
[19]	Parallel SOA-MZI	Multiple gates	Theory + Experimental	Optical logic	10
[23]	SOA interferometric	"OR"	Theoretical	PSK	100
[24]	Compact SOA multifunction	Multiple gates	Theoretical	Optical logic	100
[20]	Differential SOA-MZI	"AND" (multi-input)	Experimental + Simulation	QAM	200
[21]	Differential SOA-MZI	"OR"	Theoretical/Design	Optical logic	High speed
This work	Parallel-series SOA-MZI	"AND"-"OR" (Simultaneous)	Experimental	64-QAM	80/100

Table 4. Practical comparison of SOA-MZI-based logic gate designs in terms of energy efficiency, footprint, and cascadability

Ref.	Architecture	Energy efficiency	Footprint	Cascadability	Remark
[22]	Single SOA-MZI	Moderate	Compact	Moderate	Single-function
[19]	Parallel SOA-MZI	Moderate	Medium	Limited	Multi-gate
[23]	Interferometric	Not reported	Compact	Not discussed	"OR" gate
[24]	Compact multifunction	Favorable	Compact	Not validated	Theoretical
[20]	Differential "AND"	Moderate	Medium	Moderate	"AND" only
[21]	Differential "OR"	Moderate	Medium	Moderate	"OR" only
This work	Parallel-series SOA-MZI	Functional efficiency (multi-output)	Larger	Moderate (limited by SOA effects)	Simultaneous "AND" + "OR"

Beyond logic functionality and bit rate, the practical relevance of SOA-MZI-based optical logic systems must also be evaluated in terms of energy efficiency, footprint, and cascadability. From an energy-efficiency perspective, the proposed architecture does not aim to minimize power consumption per logic function, as it employs multiple SOA-MZI stages. However, it improves functional efficiency by enabling simultaneous "AND" and "OR" operations within a single integrated system, thereby increasing hardware utilization.

In terms of footprint, single SOA-MZI logic gates generally remain more compact than cascaded or multifunctional architectures, which require additional SOAs and optical components. Therefore, the proposed system represents a trade-off between compactness and multifunctionality.

Regarding cascadability, SOA-MZI-based systems are inherently limited by ASE noise accumulation, gain saturation, carrier recovery dynamics, and pattern-dependent effects. These factors become more critical in multistage configurations. Nevertheless, the experimental results demonstrate that the proposed architecture maintains sufficient signal quality for the considered number of stages, indicating good functional cascadability at the demonstrated scale. However, further scaling would require careful optimization to mitigate cumulative nonlinear and noise effects.

As shown in Table 4, the proposed architecture emphasizes multifunctionality and hardware reuse, while introducing trade-offs in terms of footprint and energy consumption due to the use of multiple SOA-MZI stages.

13. Conclusion

In this paper, we proposed and experimentally demonstrated a simultaneous all-optical "AND"-"OR" logic gate system based on two parallel SOA-MZI structures followed by SOA-MZI3 connected in series. The parallel SOA-MZIs generate the "AND" logic signals, while the SOA-MZI3 performs the "OR" operation, enabling a compact architecture capable of producing multiple logic functions simultaneously. The proposed system was experimentally evaluated in the optical, electrical, and temporal domains. The operation of the "AND" gates at the outputs of SOA-MZI1 and SOA-MZI2 is mainly governed by XPM, whereas the "OR" gate generated at the SOA-MZI3 output is primarily based on XGM. Several performance parameters, including optical conversion gain, ER, OSNR, and EVM, were experimentally characterized. The experimental results demonstrate that 64-QAM-modulated "AND" and "OR" signals can reach maximum bit rates of 80 Gbit/s and 100 Gbit/s, respectively, at 80 GHz. The measured EVM values remain below 8% for the "OR" signal even at 100 Gbit/s, and below 12% for the "AND" signal at 80 Gbit/s, confirming good signal quality across the entire bit rate range. Temporal analysis shows that the generated "AND" and "OR" pulses have durations of 7.7 ps and 11.1 ps, respectively, compared with the 1.3 ps pulse width of the input optical pulse source. In addition, the output beams exhibit high spatial quality with a Gaussian profile, circularity greater than 95% for the "AND" signal and 92% for the "OR" signal, and beam-propagation factors of $M^2 < 1.74$ for the "AND" signal and $M^2 < 1.5$ for the "OR" signal. Finally, power-scaling measurements and performance analysis indicate that the "OR" signal exhibits superior quality and efficiency compared with the "AND" signal, mainly due to the higher amplification provided by SOA6 in the third interferometer stage. These results demonstrate that the proposed architecture is a promising solution for high-speed all-optical signal processing in future optical communication networks.

Author contributions

H.T. and K.K. performed the principle, experiments, simulations, prepared, and reviewed the manuscript. All authors have read and agreed to the published version of the manuscript.

Data availability statement

Data underlying the results presented in this paper are not publicly available at this time, but they may be obtained from the authors upon reasonable request.

Conflicts of interest

The authors declare no conflicts of interest.

Abbreviation

ASE	Amplified Spontaneous Emission
AWG	Arbitrary Waveform Generator
BPR	Beam Propagation Ratio
CIP	Center for Integrated Photonics
DSO	Digital Sampling Oscilloscope
ER	Extinction Ratio
ESA	Electrical Spectrum Analyzer
EVM	Error Vector Magnitude
FEC	Forward Error Correction

FWHM	Full Width at Half Maximum
LNA	Low-Noise Amplifier
MZM	Mach-Zehnder Modulator
OA	Optical Attenuator
OBPF	Optical Bandpass Filter
OC	Optical Coupler
OPS	Optical Pulse Source
OSA	Optical Spectrum Analyzer
OSNR	Optical Signal-to-Noise Ratio
PC	Polarization Controller
PD	Photodiode
PIC	Photonic Integrated Circuit
PSK	Phase Shift Keying
PM	Power Meter
PS	Phase Shifter
QAM	Quadrature Amplitude Modulation
SOA	Semiconductor Optical Amplifier
SOA-MZI	SOA Mach-Zehnder Interferometer
VSA	Vector Signal Analyzer
XGM	Cross-Gain Modulation
XPM	Cross-Phase Modulation

References

[1] H. Sun, Q. Wang, H. Dong, and N. K. Dutta, "Xor performance of a quantum dot semiconductor optical amplifier-based mach-zehnder interferometer," *Optics Express*, vol. 13, no. 6, pp. 1892-1899, 2005. https://doi.org/10.1364/OPEX.13.001892.

[2] S. H. Kim, J. H. Kim, B. G. Yu, Y. T. Byun, Y. M. Jeon, S. Lee, and D. H. Woo, "All-optical nand gate using cross-gain modulation in semiconductor optical amplifiers," *Electronics Letters*, vol. 41, no. 18, pp. 1027-1028, 2005. https://doi.org/10.1049/el:20052320.

[3] H. Dong, H. Sun, Q. Wang, N. K. Dutta, and J. Jaques, "All optical logic and operation at 80 gb/s using semiconductor optical amplifier based on the mach-zehnder interferometer," *Microwave and Optical Technology Letters*, vol. 48, no. 8, pp. 1672-1675, 2006. https://doi.org/10.1002/mop.21708

[4] E. Dimitriadou and K. E. Zoiros, "On the design of reconfigurable ultrafast all-optical nor and nand gates using a single quantum-dot semiconductor optical amplifier-based mach-zehnder interferometer," *Journal of Optics*, vol. 14, no. 10, p. 105401, 2012. https://doi.org/10.1088/2040-8978/14/10/105401.

[5] S. Lee, J. Park, K. Lee, D. Eom, S. Lee, and J. H. Kim, "All-optical exclusive nor logic gate using mach-zehnder interferometer," *Japanese Journal of Applied Physics*, vol. 41, pp. 1155-1157, 2002. https://doi.org/10.1143/JJAP.41.L1155.

[6] B.-K. Kang, J. H. Kim, Y. H. Park, S. Lee, Y. M. Jhon, D. H. Woo, et al., "All-optical logic and in a soa-based mach-zehnder all-optical wavelength converter," In Proc. 13th Annual Meeting of the IEEE Lasers and Electro-Optics Society, Rio Grande, Puerto Rico, USA, Nov. 13-16, 2000. pp. 117-118. https://doi.org/110.1109/LEOS.2000.890702.

[7] M. Schilling, K. Daub, W. Idler, D. Baums, U. Koerner, E. Lach, et al., "Wavelength converter based on integrated all-active three-port mach-zehnder interferometer," *Electronics Letters*, vol. 30, no. 25, pp. 2128-2130, 1994. https://doi.org/10.1049/el:19941482.

[8] C. Joergensen, T. Durhuus, C. Braagaard, B. Mikkelsen, and K. E. Stubkjaer, "4 gb/s optical wavelength conversion using semiconductor optical amplifiers," *IEEE Photonics Technology Letters*, vol. 5, no. 6, pp. 657-660, 1993. https://doi.org/10.1109/68.219701.

[9] X. Pan, J. M. Wiesenfeld, J. S. Perino, T. L. Koch, G. Raybon, U. Koren, M. Chien, M. Young, B. I. Miller, and C. A. Burrus, "Dynamic operation of a three-port, integrated mach-zehnder wavelength converter," *IEEE Photonics Technology Letters*, vol. 7, no. 9, pp. 995-997, 1995. https://doi.org/10.1109/68.414680.

[10] H. Soto, J. D. Topomondzo, D. Erasme, and M. Castro, "All-optical nor gates with two and three input logic signals based on cross-polarization modulation in a semiconductor optical amplifier," *Optics Communications*, vol. 218, no. 4, pp. 243-247, 2003. https://doi.org/10.1016/S0030-4018(03)01202-1.

[11] J. H. Kim, Y. T. Byun, Y. M. Jhon, S. Lee, D. H. Woo, and S. H. Kim, "All-optical half adder using semiconductor optical amplifier-based devices," *Optics Communications*, vol. 218, no. 4-6, pp. 345-349, 2003. https://doi.org/10.1016/S0030-4018(03)01203-3.

[12] R. P. Webb, R. J. Manning, G. D. Maxwell, and A. J. Poustie, "40 gb/s all-optical xor gate based on hybrid-integrated mach-zehnder interferometer," *Electronics Letters*, vol. 39, no. 1, pp. 79-81, 2003. https://doi.org/10.1049/el:20030010.

[13] A. Kotb, B. Zhu, J. Cui, K. E. Zoiros, "250 gb/s all-optical xnor logic gate using quantum-dot soa-mzi: demonstration and comprehensive performance analysis," *Micromachines*, vol. 17, no. 4, p. 441, 2026. https://doi.org/10.3390/mi17040441.

[14] A. Kotb and Y. Mohamed, "Phase-shift keying modulated data signal using soa-mzi-based all-optical logic and gate at 80 gb/s," *International Journal of Optics*, vol. 2018, pp. 1-8, 2018. https://doi.org/10.1155/2018/5864530.

[15] A. Kotb, "Analysis of all-optical logic xor gate for 100 gb/s phase-shift keying modulated data signals in semiconductor optical amplifier-based mach-zehnder interferometer," *Optical and Quantum Electronics*, vol. 47, no. 5, pp. 1063-1070, 2015. https://doi.org/10.1007/s11082-014-9962-7.

[16] Q. Wang, G. Zhu, H. Chen, J. Jaques, J. Leuthold, A. B. Piccirilli, and N. K. Dutta, "Study of all-optical xor using mach-zehnder interferometer and differential scheme," *IEEE Journal of Quantum Electronics*, vol. 40, no. 6, pp. 703-710, 2004. https://doi.org/10.1109/JQE.2004.828261.

[17] M. Zhang, Y. Zhao, L. Wang, J. Wang, and P. Ye, "Design and analysis of all-optical xor gate using soa-based mach-zehnder interferometer," *Optics Communications*, vol. 223, no. 4-6, pp. 301-308, 2003. https://doi.org/10.1016/S0030-4018(03)01692-4.

[18] J.-Y. Kim, S.-K. Han, and S. Lee, "All-optical multiple logic gates using parallel soa-mzi structures," In Proc. 18th Annual Meeting of the IEEE Lasers and Electro-Optics Society, Sydney, NSW, Australia, Oct. 22-28, 2005. pp. 133-134. https://doi.org/10.1109/LEOS.2005.1547914.

[19] J.-Y. Kim, J.-M. Kang, T.-Y. Kim, and S.-K. Han, "All-optical multiple logic gates with xor, nor, or, and nand functions using parallel soa-mzi structures: Theory and experiment," *Journal of Lightwave Technology*, vol. 24, no. 9, pp. 3392-3399, 2006. https://doi.org/10.1109/JLT.2006.880593.

[20] H. Termos and A. Mansour, "All-optical three-input 'and' gate dependent on a differential modulation architecture," *Electronics*, vol. 12, no. 7, p. 1510, 2023. https://doi.org/10.3390/electronics12071510.

[21] H. Termos and A. Mansour, "High-repetition-rate femtosecond 'or' gate design in a differential soa-mzi," *Optik*, vol. 304, p. 171760, 2024. https://doi.org/10.1016/j.ijleo.2024.171760.

[22] H. Dong, H. Sun, Q. Wang, N. K. Dutta, and J. Jaques, "80 gb/s all-optical logic and operation using mach-zehnder interferometer with differential scheme," *Optics Communications*, vol. 265, no. 1, pp. 79-83, 2006. https://doi.org/10.1016/j.optcom.2006.02.045.

[23] A. Kotb, "An or gate for 100 gb/s phase-shift keying signals in semiconductor optical amplifier-based delayed interferometer," *Australian Journal of Basic and Applied Sciences*, vol. 8, no. 7, pp. 449-454, 2014.

[24] A. Kotb and C. Guo, "100 gb/s all-optical multifunctional and, nor, xor, or, xnor, and nand logic gates in a single compact scheme based on semiconductor optical amplifiers," *Optics & Laser Technology*, vol. 137, p. 106828, 2021. https://doi.org/10.1016/j.optlastec.2020.106828.

[25] H. Termos, "Study of up and down conversion technique by all optical sampling based on a soa-mzi," Ph. D. thesis, Université de Bretagne Occidentale, Brest, France, 2017.

[26] H. Termos and A. Mansour, "Ofdm signal down frequency conversion based on a soa-mzi sampling mixer using differential modulation and switching architectures," *Optik*, vol. 245, p. 167761, 2021. https://doi.org/10.1016/j.ijleo.2021.167761.

[27] H. Termos, A. Mansour, and A. Nasser, "Simultaneous up- and down-frequency mixing based on a cascaded soa-mzis link," *Applied Optics*, vol. 60, no. 27, pp. 8336-8348, 2021. https://doi.org/10.1364/AO.432179.

[28] H. Termos, A. Mansour, and A. Nasser, "Simultaneous up-conversion based on a co- & counter-directions soa-mzi sampling mixer with standard & differential modulation modes," *Photonics*, vol. 9, no. 2, p. 109, 2022. https://doi.org/10.3390/photonics9020109.

[29] H. Termos and A. Mansour, "Experimental topology of a femtosecond ring fiber cavity laser using soa-mzi for coincident ofdm dispatch," *Optics & Laser Technology*, vol. 182, p. 112076, 2025. https://doi.org/10.1016/j.optlastec.2024.112076.

[30] H. Termos and A. Mansour, "Concurrent m-qam transmission performance assessment in a combined four soa-mzis arrangement," *Optics and Lasers in Engineering*, vol. 176, p. 108110, 2024. https://doi.org/10.1016/j.optlaseng.2024.108110.

[31] H. Termos, A. Mansour, and M. Ebrahim-Zadeh, "Establishment of an electro-optical mixing design on a photonic soa-mzi using a differential modulation arrangement," *Sensors*, vol. 23, no. 9, p. 4380, 2023. https://doi.org/10.3390/s23094380.

[32] G. P. Agrawal, *Fiber-Optic Communication Systems*, 4th ed. Hoboken, NJ, USA: Wiley, 2010.

[33] G. P. Agrawal and N. A. Olsson, "Self-phase modulation and spectral broadening of optical pulses in semiconductor laser amplifiers," *IEEE Journal of Quantum Electronics*, vol. 25, no. 11, pp. 2297-2306, 1989. https://doi.org/10.1109/3.42059.

[34] B. Mukherjee, *Optical WDM Networks*. New York, NY, USA: Springer, 2006. https://doi.org/10.1007/0-387-29188-1.

[35] T. Houbavlis, K. E. Zoiros, G. Kanellos, and C. Tsekrekos, "Performance analysis of ultrafast all-optical boolean xor gate using semiconductor optical amplifier-based mach-zehnder interferometer," *Optics Communications*, vol. 232, pp. 179-199, 2004. https://doi.org/10.1016/j.optcom.2003.12.062.

[36] CIP Technologies, "Twin 40g/s 2r optical regenerator (preliminary datasheet)," [online]. Available https://www.ciphotonics.com. [Accessed Jun. 25, 2025].

[37] A. Fernandez, L. Chao, and J. W. D. Chi, "All-optical clock recovery and pulse reshaping using semiconductor optical amplifier and dispersion compensating fiber in a ring cavity," *IEEE Photonics Technology Letters*, vol. 20, no. 13, pp. 1148-1150, 2008. https://doi.org/10.1109/LPT.2008.925186.

[38] V. Stasyuk, "Test data and operation manual of ultrafast optical clock," Pritel, Inc., [online]. Available https://www.pritel.com. [Accessed Jun. 25, 2025].

[39] D. Wright, "Beam widths of a diffracted laser using four proposed methods," *Optical and Quantum Electronics*, vol. 24, no. 9, pp. S1129-S1135, 1992. https://doi.org/10.1007/BF01588611.

[40] A. E. Siegman, "How to (maybe) measure laser beam quality," in *Proc. Diode Pumped Solid State Lasers: Applications and Issues*, M. Dowley, Ed. Washington, DC, USA: Optica Publishing Group, paper MQ1, 1998. https://doi.org/10.1364/DLAI.1998.MQ1.

[41] R. Schmogrow, B. Nebendahl, M. Winter, A. Josten, D. Hillerkuss, S. Koenig, J. Meyer, M. Dreschmann, M. Huebner, C. Koos, J. Becker, W. Freude, and J. Leuthold, "Error vector magnitude as a performance measure for advanced modulation formats," *IEEE Photonics Technology Letters*, vol. 24, pp. 61-63, 2012. https://doi.org/10.1109/LPT.2011.2172405.

[42] D.-N. Nguyen, J. Bohata, J. Spacil, D. Dousek, M. Komanec, S. Zvanovec, Z. Ghassemlooy, and B. Ortega, "M-qam transmission over hybrid microwave photonic links at the k-band," *Optics Express*, vol. 27, pp. 33745-33756, 2019. https://doi.org/10.1364/OE.27.033745.

[43] M. A. Mestre, H. Mardoyan, C. Caillaud, R. Rios-Müller, J. Renaudier, P. Jennevé, and F. Blache, "Compact inp-based dfb-eam enabling pam-4 112 gb/s transmission over 2 km," *Journal of Lightwave Technology*, vol. 34, pp. 1572-1578, 2016. https://doi.org/10.1109/JLT.2015.2508677.

[44] Y. Cai, N. Ramanujam, J. M. Morris, T. Adali, G. Lenner, A. B. Puc, and A. Pilipetskii, "Performance limit of forward error correction codes in optical fiber communications," In Optical Fiber Communication Conference and Exhibit, Anaheim, CA, USA, Mar. 17-22, 2001. https://doi.org/10.1109/OFC.2001.927308.

[45] M. J. Connelly, *Semiconductor Optical Amplifiers*. Boston, MA, USA: Springer-Verlag, 2002. https://doi.org/10.1007/b101817.

[46] J. Mørk, A. Mecozzi, and G. Eisenstein, "The modulation response of semiconductor optical amplifiers," *IEEE Journal of Selected Topics in Quantum Electronics*, vol. 5, no. 3, pp. 851-860, 1999. https://doi.org/10.1109/2944.788459.

[47] K. E. Zoiros, T. Houbavlis, and G. T. Kanellos, "Theoretical analysis and performance investigation of ultrafast all-optical boolean gates using soa-mzi structures," *Optics Communications*, vol. 223, pp. 113-130, 2003. https://doi.org/10.1016/j.optcom.2005.07.059.